Annals of Nuclear Energy 191 (2023) 109918

Contents lists available at ScienceDirect

Annals of Nuclear Energy

journal homepage: www.elsevier.com/locate/anucene

Modal analysis of lead-bismuth eutectic flow in a single wire-wrapped rod channel

Xielin Zhao [a], Qian Cheng [a], Xiaofei Yu [b], Qian Huang [b], Ke Zhang [b], Zhipeng Feng [b,*], Jinxiong Zhou [a,*]

[a] State Key Laboratory for Strength and Vibration of Mechanical Structures and School of Aerospace, Xi'an Jiaotong University, Xi'an 710049, People's Republic of China

[b] Key Laboratory of Nuclear Reactor System Design Technology, Nuclear Power Institute of China, Chengdu 610200, People's Republic of China

ARTICLE INFO

Keywords:
Lead-bismuth eutectic
Wire-wrapped rod fuel assembly
Dynamic mode decomposition
RANS
Reduced-order modeling

ABSTRACT

The thermal-hydraulics as well as flow-induced vibration of wire-wrapped rod bundles calls for accurate and efficient liquid metal flow simulation and prediction, yet it remains a challenge due to the complex geometries and high Reynolds number flow in wire-wrapped rod channel. Previous efforts towards this goal exclusively adopts full-order modeling (FOM), which is prohibitively computation-intensive. This work reports the first reference on modal analysis of the turbulent lead-bismuth eutectic (LBE) flow in a single wire-wrapped rod channel by a data-driven dynamic mode decomposition (DMD) method. The spatio-temporal data of fluid velocities and pressure were modeled and collected by using the Reynolds-averaged Navier–Stokes equations (RANS) approach with stress-omega RSM turbulence model. Modal analysis was performed over the snapshot matrices and DMD modes and corresponding eigenvalues were calculated. The DMD modes and eigenvalues were then used to construct a reduced-order modeling (ROM) system for fast fluid field reconstruction and short-term forecasting. The correctness and feasibility of the method was demonstrated and compared with ground-truth CFD simulation results. Our method offers a fast and reliable approach for ROM of turbulent flow in wire-wrapped rod fuel assemblies. We publicize all the data and codes via https://github.com/XJTU-Zhou-group/Wire-wrapped-fuel-pin-CFD-DMD.

1. Introduction

Lead-bismuth eutectic (LBE) has been widely recognized as one of the candidate coolants for next-generation liquid metal-based fast nuclear reactors. However, several key issues need to be resolved with regard to material corrosion, structural and seismic design, oxygen and polonium control, and thermal hydraulics, before LBE fast reactors can be counted as a reliable option for future application (Alemberti et al., 2014). Compared with water, LBE has a high density and a very low Prandtl number, leading to its heat transfer and thermal hydraulics quite different from the water cooled vessel and becoming a primary concern for design support and safety analysis of LBE-based reactors. Roelofs (2020) described an excellent review on the state-of-the-art and future perspectives of liquid metal thermal hydraulics. Identified problems include liquid metal heat transfer, fluid–structure interaction, fuel assembly thermal hydraulics, coolant solidification, 3D system modeling and validation (Roelofs, 2020; Merzari et al., 2021).

As for thermal hydraulics of an LBE fuel assembly, a special concern is the adoption of wire-wrappers in lieu of grids commonly used in pressurized water reactor (PWR) fuel assemblies. Wire-wrapped fuel pins generate a comparatively larger transverse flow and increase the possibility of flow-induced vibrations (FIV) (Brockmeyer et al., 2020). In recent years, due to the peculiarity of LBE, extensive thermal-hydraulic and FIV experimental tests have been performed on the LBE-cooled, wire-wrapped fuel assembly of MYRRHA in large-scale LBE experimental test facilities (Van Tichelen et al., 2020; Bovati et al., 2022). The fuel assembly pressure drop and FIV characteristics were tested with a full-scale 127-pin mock-up test section by Kennedy et al. (2015). Experimentally measuring LBE flows in pin bundle channels as well as vibration of a wire-wrapped rod is costly, difficult and sometimes inaccessible due to the narrow gap between wire and adjacent rod, sliding of wire and the possible contacts. Resort is thus made to perform computational fluid dynamics (CFD) simulation and computational structure dynamics without using empirical force coefficients, identifying and elucidating phenomena and the underlying mechanisms for the future design of wire-wrapped fuel pin bundles.

* Corresponding authors.
E-mail addresses: fengzhipengchn@163.com (Z. Feng), jxzhouxx@mail.xjtu.edu.cn (J. Zhou).

https://doi.org/10.1016/j.anucene.2023.109918
Received 19 November 2022; Received in revised form 19 March 2023; Accepted 8 May 2023
Available online 17 May 2023

Nomenclature

$\bar{U}^+, \bar{V}^+, \bar{W}^+$	Time average dimensionless velocity; normalized by U_τ
μ	Dynamic viscosity kg/(m s)
ρ	Density kg/m^3
τ_ω	Statically averaged wall shear stress N/m^2
D	Diameter of rod mm
d	Diameter of wire mm
L	Wire (wrapping) pitch mm
L_g	Gap between wire and rod mm
P	Static Pressure N/m^2
Re	Reynolds number
S^+	Non-dimensionalized length
U, V, W	Velocity m/s
U^+, V^+, W^+	Dimensionless velocity; normalized by U_τ
U_τ	Friction velocity m/s

Cadiou and Saxena (2015) performed a steady RANS simulation of 217-pin wire-wrapped bundle for sodium-cooled fast reactors. Shams et al. (2018) utilized STAR-CCM+ and performed a pseudo-direct numerical simulation (DNS) based on the multipurpose hybrid research reactor for high-tech application, MYRRHA, fuel design. The LBE flow in a single wire-wrapped rod channel was simulated with periodic boundary conditions. The mesh used has a DNS quality up to 42 million polyhedral meshes for a low velocity case with Re=7015, and a second-order scheme is used. The study provides a high fidelity reference database for a wire-wrapped fuel assembly, and serves as a benchmark to validate other low order turbulence model results. Dovizio et al. (2020) performed validation of steady RANS simulations of LBE flow for various fuel assemblies. The RANS results of a single wire-wrapped tube was validated against pseudo-DNS results, the 7-pin bundle results were compared with experimental results, and the 61-pin bundle RANS results were checked by LES results. The overall conclusion is that the RANS approach is able to provide reasonably good results. The adoption of a wall resolved mesh and nonlinear models are suggested. Bovati et al. (2021) used RANS approaches to investigate the flow behavior of liquid metal sodium in a 61-pin wire-wrapped bundle for a range of Reynolds numbers from 1270 to 100000. The internal subchannel velocity results were compared with experimental data and LES results and found in reasonable agreement. Merzari et al. (2016) adopted Nek5000 to carry out LES simulation of LBE flow in a 7-pin wire-wrapped bundle. They also performed a code-to-code comparison, and found that good agreement is attainable in terms of velocity and cross flows.

Compared with the above-mentioned intensive studies on CFD simulation of wire-wrapped pin bundle, study on fluid–structure interaction (FSI) of wire-wrapped rod bundle is very limited and scarce in literature. Inherently, the experimental data on FSI of wire-wrapped fuel pin bundle subjected to LBE flow is hard to obtain. De Pauw et al. (2016) measured the fuel assembly vibration in a LBE cooled installation by using optical fiber sensors. Nixon (2018) developed a new method for monitoring the FIV of a cylinder, utilizing a single, high-resolution distributed strain sensor in a helical configuration, and demonstrated the ability to measure the simultaneous dynamic response of adjacent pins in pin bundle flow tests. For numerical simulation on FSI of wire-wrapped bundle, De Santis and Shams (2019) analyzed the FIV and static deformation of a single wire-wrapped fuel rod by the two-way coupling FSI module in STAR-CCM+, and accounted for the effects of wire spacers and working fluids. Brockmeyer at Brockmeyer et al. (2020) carried out flow-induced vibration for a 7-pin wire-wrapped fuel pin bundle by coupling Nek5000, a spectral element LES solver with a finite element solver. In order to obtain force history data for the 2.63 helical pitch structure, a scheme was developed to artificially generate force history from the power spectrum density (PSD) of the one-pitch CFD simulation forces. Dolfen et al. (2022) conducted a multi-stage approach to simulate FIV of a 7-pin wire-wrapped fuel pin bundle.

CFD simulation and FSI simulation of wire-wrapped pin bundle is prohibitively computation-intensive. All above-mentioned CFD simulation adopt full order modeling (FOM), which is highly time-consuming and resource-exhausting. Recently, Yildiz et al. (2019) performed LES simulation of the flow in a helical coil steam generator, then employed proper orthogonal decomposition (POD) to reveal the coherent structures in the flow and their evolution. This offers an efficient way to perform ROM of complex flows. As for flow in a wire-wrapped rod channel, no such efforts have been conducted towards modal analysis and ROM, to our best knowledge. Two widely used mode decomposition methods are the POD method and the dynamic mode decomposition (DMD) method. These two methods share many similarities in terms of snapshot matrix construction, mode calculation and mode summation. DMD can not only calculate modes of the accumulated data as POD does, but also gives the frequencies as well as the growth or decay rate of the time-series data. The DMD method originated in the fluid community as a method to perform modal analysis of fluid and to explore spatio-temporal coherent structures (Kutz et al., 2016). Schmid and Sesterhenn (2008) and Schmid (2010) gave the widely adopted DMD algorithm and demonstrated its ability to analyze high-dimensional fluids data. Mezić (2005, 2013), Mezić and Banaszuk (2004) and Rowley et al. (2009) uncovered the connection between DMD and Koopman operator theory. Tu (2013) extended the classical definition of the DMD algorithm which is limited to sequential time-series data to a more general algorithm that works for non-sequential time-series. A major promise of DMD in fluids is the ability to synthesize data from simulations or experiments into accurate and computationally tractable ROMs. Other advances include the use of DMD to create a hybrid ROM for future-state prediction. Zhao et al. (2022) proved that DMD works well for both data reconstruction and future-state prediction, in terms of either free surface profiles or the sloshing pressure exerted on the rigid wall. Since DMD introduction, has spawned various extensions, generalizations, and improvements. Schmid (2022) and Chen et al. (2012) summarized and categorized variants of DMD variants. Naderi et al. (2019) presented hybrid DMD method for analysis and forecasting of unsteady fluid flows over moving structures such as rotating cylinder, oscillating airfoil, and Savonius wind turbine. DMD defined as $\mathbf{x}_{k+1} = \mathbf{A}\mathbf{x}_k$ can be thought of as a multivariate regression of the dynamics, where $\mathbf{x}_j$ is the vector of variables at time t_j, $\mathbf{A}$ is the similar matrix (linear term). If the mean of $\mathbf{X} = [\mathbf{x}_1 \quad \mathbf{x}_2 \cdots \mathbf{x}_{n-1}]$ is not zero, then the DMD model would be improved as $\mathbf{x}_{k+1} = \mathbf{A}\mathbf{x}_k + \mathbf{C}$, where $\mathbf{C}$ is the companion matrix (bias term). Hirsh improved the companion matrix method proposed by Chen et al. (2012) and proved that centering (mean-subtracted) data improves the performance of DMD. Further examples and theoretical results on time-delay embedding and the Hankel DMD of Koopman analysis have been given by Brunton et al. (2017) and Kamb et al. (2020); they convincingly demonstrated that linear time-delayed models are an effective and efficient tool to capture nonlinear and chaotic dynamics. This paper focus on the LBE flow in a single wire-wrapped rod channel, which does not involve moving boundary problem and chaos phenomenon, therefore standard DMD was adopted for modal analysis and ROM simulation.

In light of the above-mentioned practices, this paper presents the DMD modal analysis of turbulent LBE flow in a single wire-wrapped rod channel. The polyhedral meshing technology was adopted, and time-series data was collected from CFD simulation based on RANS approach. The CFD data were velocity results based on a RANS model were validated against the pseudo-DNS results and found agree reasonably well. The coherent structures of the LBE flow were obtained and then used for data reconstruction and prediction in an efficient way

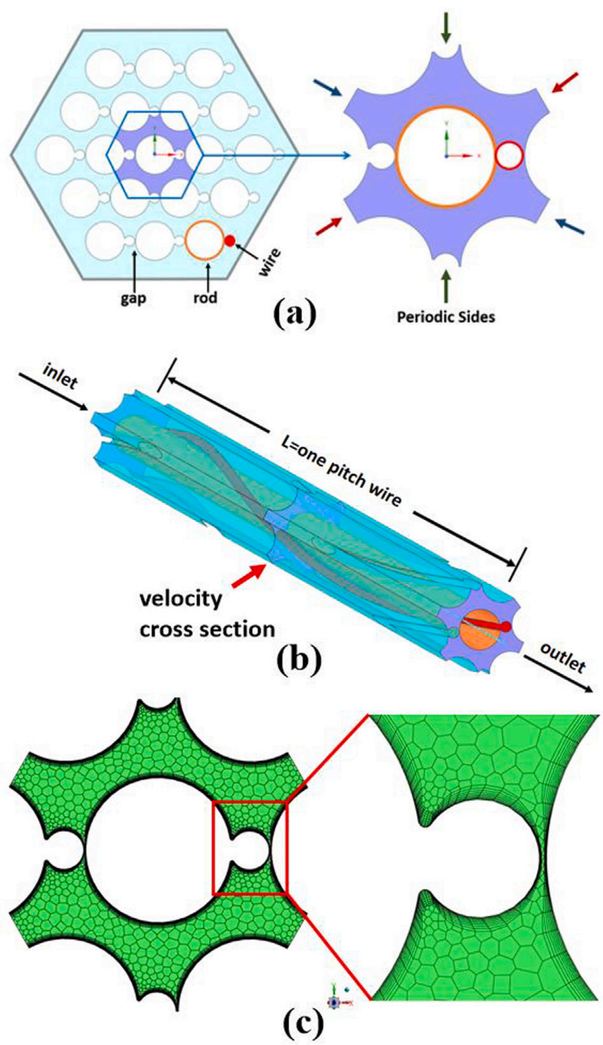

Fig. 1. Illustration of the physical and computational model for axial flow in a single wire-wrapped rod channel. (a) The cross-sectional view of a hexagonal lattice of pins and the representative unit cell of wire-wrapped rod. Three transverse pairs of boundaries indicated by the arrows in the unit cell were enforced with periodic boundary conditions. (b) Isometric view of the computational domain of a single wire-wrapped rod channel. Periodic boundary conditions were also imposed on the surfaces of inlet and outlet that are one-pitch apart. (c) Cross-sectional view of the polyhedral meshes and a close-up of a localized meshing.

of ROM modeling. Particular emphasis is placed on the distribution of static pressure, and DMD results agree well with ground-truth CFD results. Our efforts open an avenue for modal analysis and ROM of turbulent flow in wire-wrapped pin bundle, which is necessary for thermal-hydraulic and FSI study on fuel assembly for fast reactors design.

2. Methodology

The DMD method explicitly assumes that the system under investigation is linear:

$$\mathbf{x}_{k+1} = \mathbf{A}\mathbf{x}_k \tag{1}$$

where $\mathbf{x}_j = \mathbf{x}(t_j)$ and $\mathbf{A} \in \mathbb{R}^{n\times n}$. In DMD, two data matrices are assembled:

$$\mathbf{X} = [\mathbf{x}_1 \quad \mathbf{x}_2 \cdots \mathbf{x}_{n-1}], \mathbf{X}' = [\mathbf{x}_2 \quad \mathbf{x}_3 \cdots \mathbf{x}_n] \tag{2}$$

where n is the total number of snapshots, and $\mathbf{X}'$ is only a time-shifted matrix of $\mathbf{X}$. Combining Eqs. (1) and (2) yields

$$\mathbf{X}' = \mathbf{A}\mathbf{X} \tag{3}$$

this gives

$$\mathbf{A} = \mathbf{X}'\mathbf{X}^{\dagger} \tag{4}$$

where † is the Moore–Penrose pseudo-inverse. Performing singular value decomposition (SVD) of $\mathbf{X}$ gives

$$\mathbf{A} \approx \mathbf{X}'\tilde{\mathbf{V}}\tilde{\boldsymbol{\Sigma}}^{-1}\tilde{\mathbf{U}}^{*} \tag{5}$$

where $\boldsymbol{\Sigma}$ is the singular values matrix, tildes indicate low-rank approximations for computing the pseudo-inverse, and $*$ denotes the conjugate transpose. A low-rank approximation, $\tilde{\mathbf{A}}$, can be obtained by projecting $\mathbf{A}$ onto the POD modes $\tilde{\mathbf{U}}$:

$$\tilde{\mathbf{A}} = \tilde{\mathbf{U}}^{*}\mathbf{A}\tilde{\mathbf{U}} = \tilde{\mathbf{U}}^{*}\mathbf{X}'\tilde{\mathbf{V}}\tilde{\boldsymbol{\Sigma}}^{-1} \tag{6}$$

The eigendecomposition of $\tilde{\mathbf{A}}$ is defined by

$$\tilde{\mathbf{A}}\mathbf{W} = \mathbf{W}\boldsymbol{\Lambda} \tag{7}$$

where $\mathbf{W}$ are eigenvectors and $\boldsymbol{\Lambda}$ is a diagonal matrix containing the corresponding eigenvalues λ_k.

The eigenvalues of $\tilde{\mathbf{A}}$ and $\mathbf{A}$ are equivalent and the eigenvectors are related through a transformation (Kutz et al., 2016). The eigenvectors of $\mathbf{A}$ are called DMD modes, and are given by the following relationship:

$$\boldsymbol{\Phi} = \mathbf{X}'\tilde{\mathbf{V}}\tilde{\boldsymbol{\Sigma}}^{-1}\mathbf{W} \tag{8}$$

Once the DMD modes are available, the projected future solution can be constructed for all time in the future. The approximate solution at all future times is given by

$$\mathbf{x}(t) = \sum_{k=1}^{r}\phi_k e^{\omega_k t} b_k = \boldsymbol{\Phi} e^{(\Omega t)}\mathbf{b} \tag{9}$$

where r is the number of the DMD modes, and $\Omega = diag(\Omega)$ is a diagonal matrix whose entries are the eigenvalues $\omega_k = \ln \lambda_k / \triangle t$, b_k is the initial amplitude of each mode, and $\mathbf{b} = \boldsymbol{\Phi}^{-1}\mathbf{x_1}$ is a vector of the coefficients b_k. The b_k denotes the amplitude of the kth mode, which represents the modal contribution on the initial snapshot $\mathbf{x_1}$. For a standard DMD approach (Taira et al., 2017), DMD modes are ordered by their amplitudes (entries of vector $\mathbf{b}$).

3. Methodology validation

Fig. 1 illustrates the physical and the computational model of the problem of interest. Fig. 1(a) is the cross-sectional view of a hexagonal lattice of wire-wrapped fuel pins. The inset is a close-up of a representative unit cell marked in violet. Three pairs of boundaries in transverse direction indicated by the arrows in the unit cell were enforced with periodic boundary conditions. Fig. 1(b) is the isometric view of the computational domain of a single wire-wrapped rod channel. Relevant geometrical parameters of the fuel assembly are summarized in Table 1. Periodic boundary conditions were imposed at the inlet and outlet. Great attention was paid to the meshing of the complex flow domain. The recent polyhedral meshing technology in Fluent-Meshing was used for current study, and mesh refinement is carried out by leveraging the body of influence (BOI) size function available in Fluent-Meshing. In the near wall region, a structured prism layer mesh was generated to correctly capture the near wall high flow gradients, with the value of $Y+$ close to 1 for the first layer cell height less than 2×10^{-5} m. Fig. 1(c) shows the cross-sectional view of the meshing and the local details. All together, three different meshes of 4.8, 8, 14 and 16 million cells, were generated for mesh-independence check, as summarized in Table 2. Eventually, the mesh with 14 million cells were selected for the following CFD simulations. The commercial CFD solver, Fluent, is used, and the simulation details are summarized as follows. The density

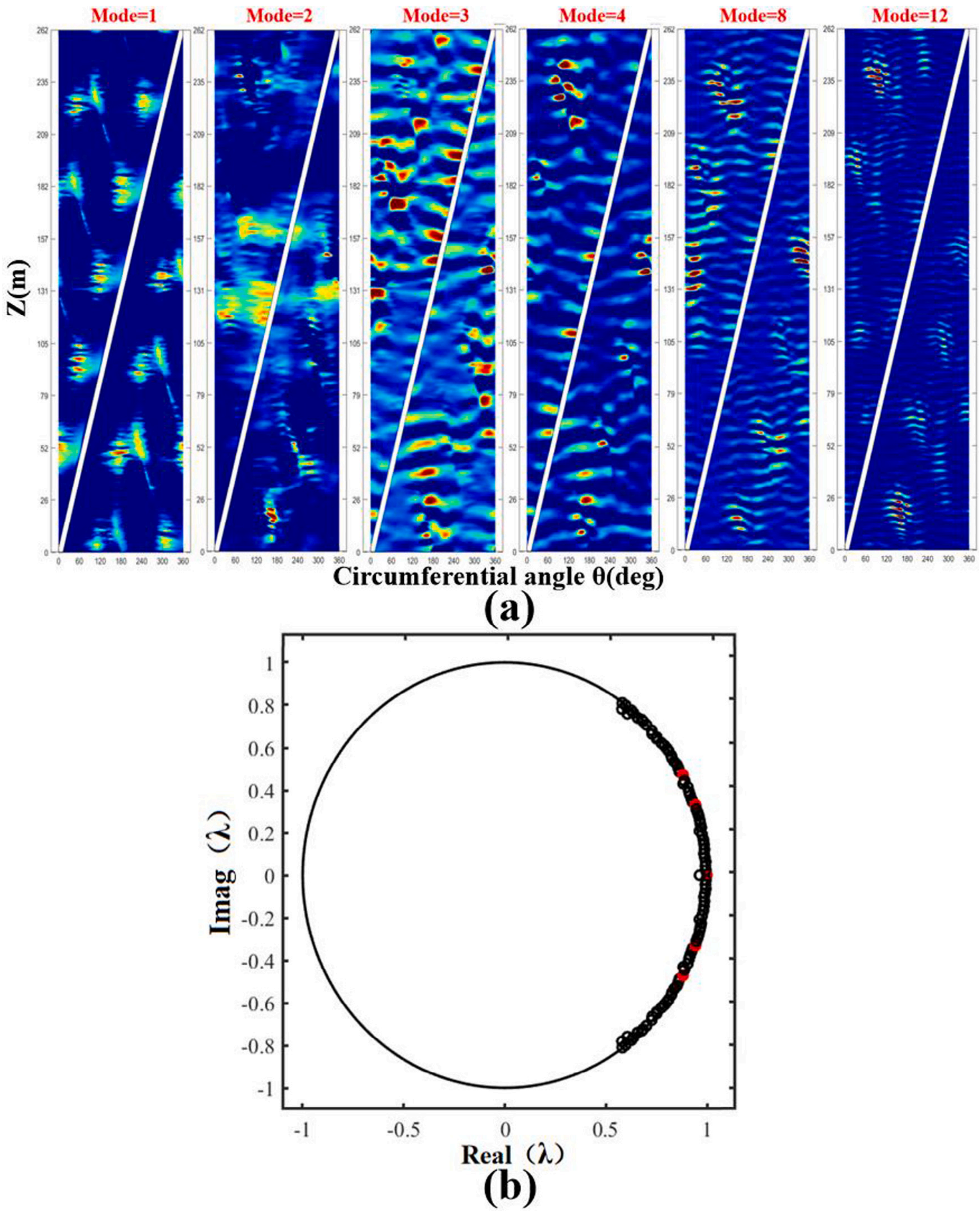

Fig. 2. DMD modes and corresponding eigenvalues obtained through decomposition of snapshot matrix collected from spatio-temporal pressure data. (a) Representative modes given in the circumferentially expanded view of the wire-wrapped rod. The narrow white strip is the projection of the helical wire on the circumferentially expanded rod surface. (b) Complex plane plot for the eigenvalues.

of LBE ρ is 10285 $\mathrm{kg/m^3}$, the dynamic viscosity μ is 1.69×10^{-3} $\mathrm{kg/(m\ s)}$, and temperature is 340 °C, in accordance with Shams et al. (2018). The flow is driven by a fixed mass flow rate of 0.2335 kg/s with a bulk velocity about 0.305 m/s in axial direction. *Re* based on the hydraulic diameter is about 7015. The boundary conditions of wires and rods were set as no-slip wall. The stress-omega RSM turbulence model based on the omega equation and LRR model (Wilcox et al., 1998) was used, and it is unnecessary to use wall functions to resolve the near-wall sublayer. The fluid flow equations were solved by the SIMPLE algorithm with second-order upwind scheme. The time step was set to 5×10^{-5} s, ensuring that Courant–Friedrichs–Lewy (CFL) number was less than 1. The CFL number is defined by $\mathbf{C} = \frac{U\Delta t}{\Delta x}$, where U is the velocity, Δt is the time step and Δx is the grid size in the streamwise direction. The number of maximum iterations per time step was set to 20, and the adopted convergence criterion was the residual of the continuity equation and the momentum equation less than 1×10^{-5}.

Data processing and assembling is crucial for implementation. We programmed MATLAB codes for data extracting from Fluent, snapshot constructing and DMD decomposition, and then post-processing with interface with Tecplot. In fluent, data extracting can be easily realized by using output module and selecting data domain. The options, EXPORT DURING CALCULATION can export variable data in interval

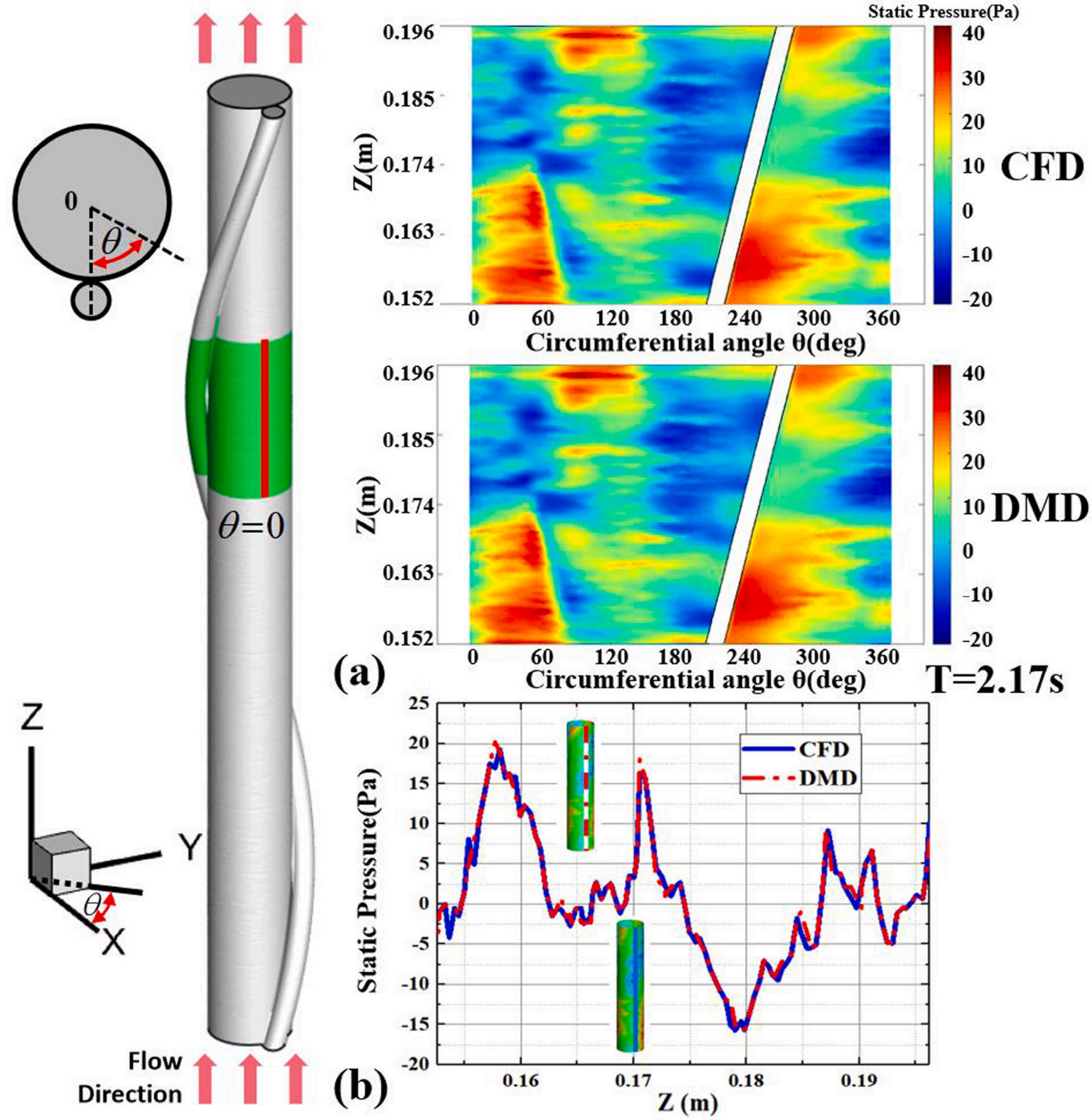

Fig. 3. Comparison of pressure data from CFD simulation and DMD reconstruction at t=2.17 s. The inserted schematic shows a full pitch wire-wrapped rod and one-sixth of it marked in green color. The cylinder coordinates used are also given. (a) Pressure contours given on the circumferentially expanded rod surface. (b) The line distribution of static pressure over the course of the red straight line marked in (a).

Table 1
Dimensions of the infinite wire-wrapped rod bundle based on the MYRRHA design (De Bruyn et al., 2013).

Dimensions for MYRRHA Design	Values (Units)
Diameter of rod	6.55 (mm)
Diameter of wire	1.75 (mm)
Wire (wrapping) pitch	262 (mm)
Pitch to diameter ratio (P/D)	1.279

Table 2
Calculated friction velocity U_τ over the main rod and the relative discrepancies for the different meshes.

Mesh (million)	Calculated friction velocity U_τ	relative discrepancies (%)
4.8	0.019935	0.28
8	0.01998	0.05
14	0.01999	0
16	0.01999	0

Δt_{snap}, the FILE TYPE can set the format of output data as .plt which contains the variable data and the information of mesh units. The unsteady LBE flow reaches a steady state after an elapsed time of 2.0s, and the simulation terminated at t=3.0 s. The simulation process took 20 days, and it was run on computer cluster with 64 processors, each having a speed of 2.4 GHz resulting in a total computational time of thirty thousands core hours. In the following discussions and comparisons, we use dimensionless velocities, which are defined as $U^+ = U/U_\tau$, where U is the local velocity and U_τ is the wall friction velocity. The U_τ is defined as $U_\tau = \sqrt{\tau_w/\rho}$, where τ_w is the statistically averaged wall shear stress. The τ_w and U are easy to be obtained from Fluent, so the dimensionless velocity U^+ could be calculated in this way. Three dimensionless velocities, U^+, V^+, W^+, of the cross section marked in Fig. 1(b), and the static pressure (P) on the surface of wire-wrapped fuel pin from t=2.0 s to t=2.6 s were assembled to form four snapshot matrices with data output time step Δt_{snap}=0.002 s. Four

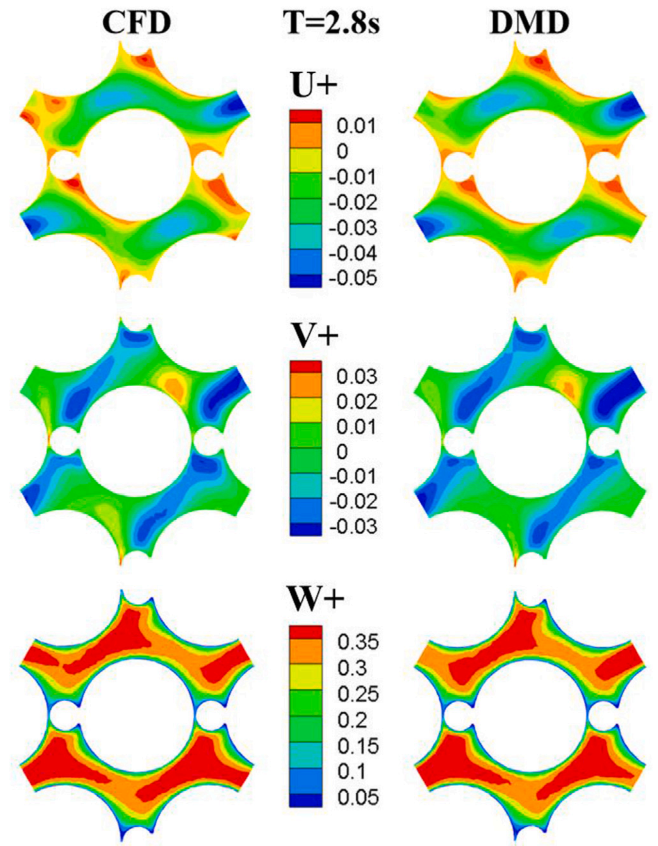

Fig. 4. Cross-sectional views of three dimensionless velocity contours. The cross-section is taken from the cross section marked in Fig. 1(b) and the time moment at t=2.8 s.

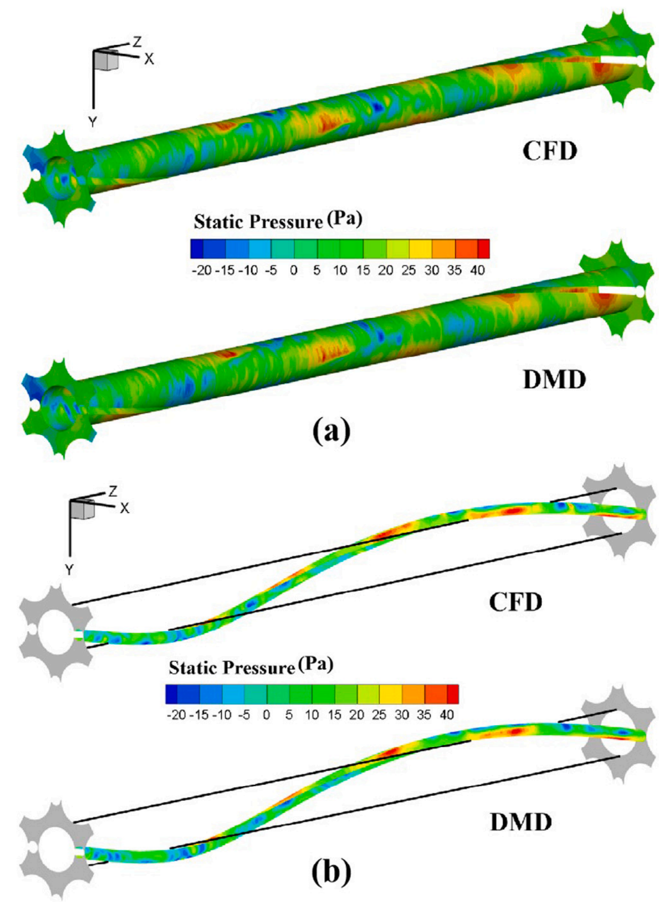

Fig. 5. Comparison of pressure contours at t=2.8 s obtained from CFD simulation and DMD prediction. Contours are given on the surface of the rod (a) and the wire (b), respectively.

snapshot matrices corresponding to U^+, V^+, W^+ and P are arranged in such a way that the number of rows equals to the number of spatial points saved per time snapshot and the number of columns equals to the number of snapshots taken, all in an increasing order. The unseen data from t=2.6 s to t=3. s were used for testing of DMD prediction. The DMD process took few minutes, compared with the time cost of CFD calculation, it can be neglected. In this way, the DMD method saves 13.3% of the time cost (the dimensionless velocity and static pressure predicted by DMD from t=2.6 s to t=3.0 s). All the data and codes used here could be downloaded via https://github.com/XJTU-Zhou-group/Wire-wrapped-fuel-pin-CFD-DMD.

Once the snapshot matrices were constructed as described previously, DMD decomposition was performed with respect to each snapshot matrix, and the corresponding DMD modes and eigenvalues were obtained. Accordingly, one can attain DMD modes for three velocities in x, y and z directions, along with DMD mode for pressure. Fig. 2(a) presents the DMD modes obtained by decomposing static pressure snapshot matrix, and the corresponding eigenvalues are plotted in the complex plane of real versus imaginary part of eigenvalues. The DMD modes in Fig. 2(a) reveal the coherent structures of LBE flow in a wire-wrapped rod channel, and characterize the spatial distribution of the coherent structures. The complex plane plot of the eigenvalues, Fig. 2(b) with the unitary circle plotted by the black solid line, indicates the growth or decay of each mode: all eigenvalues fall in the vicinity of the unit circle implying that all these modes are stable. When the DMD modes are at hand, one can easily perform data reconstruction and future-state prediction. Choosing an arbitrary moment in the range of time interval for snapshot construction, eg. t=2.17 s, without loss of generality, the reconstructed pressure data is presented in Fig. 3, together with CFD data for comparison. To quantify the prediction quality, we used the coefficient of determination (R^2) over all spatial locations which is defined in Eq. (10). R^2 is usually between zero to one,

$$R^2 = 1 - \frac{\sum_{i=1}^{m}(y_i - \hat{y}_i)^2}{\sum_{i=1}^{m}(y_i - \bar{y}_i)^2} \tag{10}$$

where y_i is the real data (CFD data), $\hat{y}_i$ represents the predicted data, and $\bar{y}_i$ is the mean of the real data. In addition, m is the number of samples. Fig. 3(a) shows the circumferentially expanded view of pressure contours evaluated over the green area marked in the inserted schematic of the wire-wrapped rod. The axial distance of the green area is one-sixth of the pitch, with Z coordinate from 152.6 mm to 192.6 mm. Fig. 3(b) plots the line distribution of static pressure along the red line $\theta = 0°$ marked in the schematic of Fig. 3(a). Result in Fig. 3 confirm that reconstructed data from DMD agrees well with the data from CFD (the R^2 is 0.986 which is satisfactory), either in terms of the distribution of high/low pressure in Fig. 3(a) or the spatial pressure profile in Fig. 3(b). Note that the flow direction in Fig. 3 is from bottom to top, the area in front of the wire exhibits higher pressure while the area behind the wire has lower pressure, similar to the pressure distribution of flow passing a cylinder or a bluff body. Which means the liquid LBE flow pass the wire, the higher pressure area represents the leading region in front of the wire, and the lower pressure area represents the wake region behind the wire. Compared with the DMD reconstruction pressure plot in Fig. 3(a), the DMD method can obtain the characteristic of flow pressure field in wire-wrapped rod channel. The DMD method is equally useful for predicting flow velocity.

DMD works well not only for data reconstruction, but also for future-state prediction. Fig. 4 shows the cross-sectional views of dimensionless velocities in three directions, U^+, V^+, W^+, respectively. The

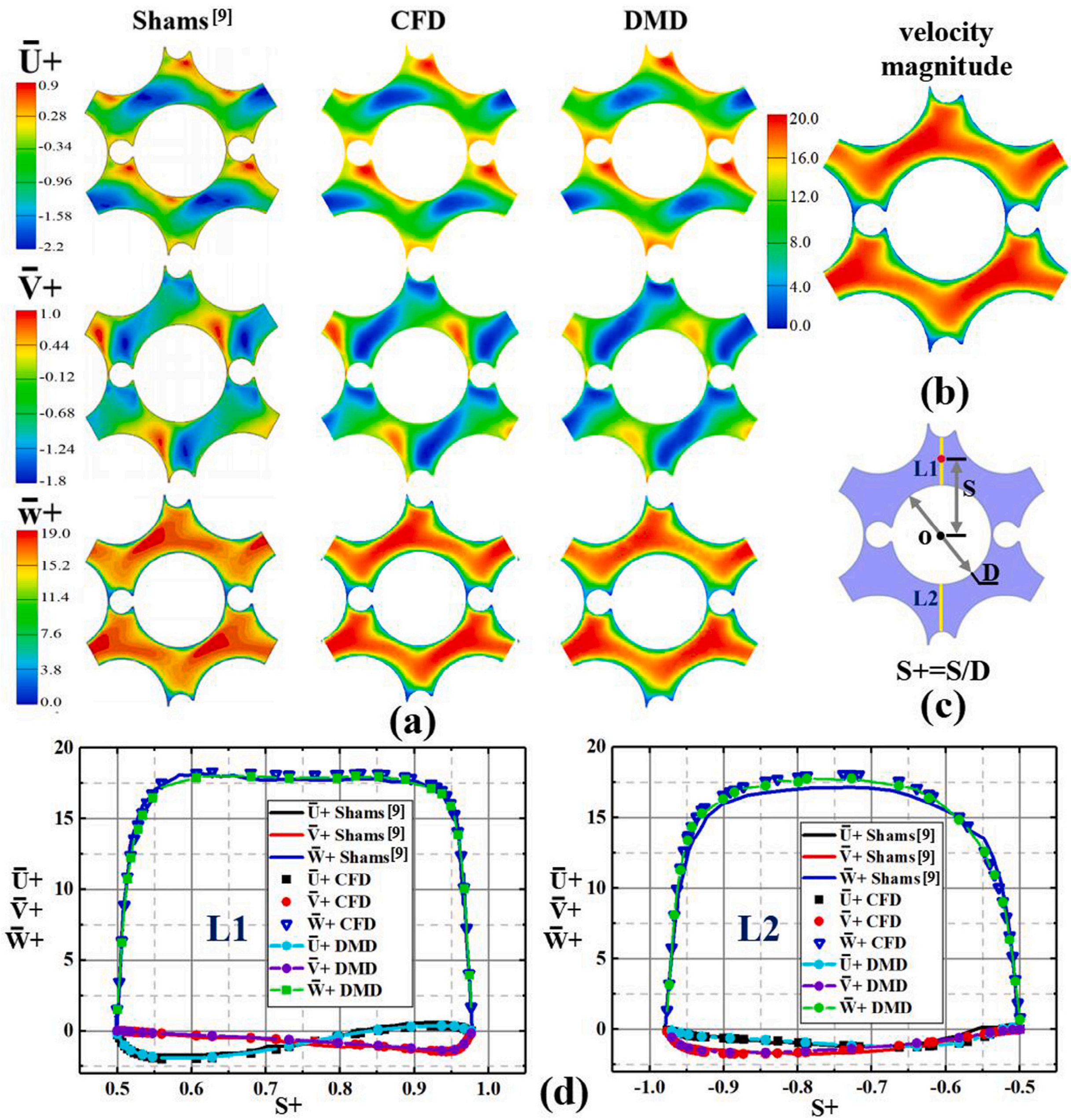

Fig. 6. Time averaged dimensionless velocities obtained by three different approaches. (a) Cross-sectional views of dimensionless time averaged velocity contours given by pseudo-DNS (Shams et al., 2018) (left, reprinted with permission), RANS CFD (middle) and DMD (right). (b) Time averaged velocity magnitude. (c) The cross section used for comparison and two lines, L_1 and L_2, along which spatial distribution of velocities are extracted and compared. (d) Velocity profiles given by three different approaches.

R^2 of U^+, V^+, W^+ at $t = 2.8$ s are 0.9376, 0.9499, 0.997, respectively, which are acceptable. The cross section in Fig. 4 is the one marked in Fig. 1(b), in the middle of the one-pitch wire-wrapped rod. The time instant in Fig. 4 is t=2.8 s, beyond the time interval from t=2.0 s to t = 2.6 s for snapshot collection. The prediction for velocities was attained by performing DMD decomposition of three velocity snapshot matrices, and then forecasting according to Eq. (9). This process can definitely be repeated for pressure snapshot data, and the results are presented in Fig. 5 for the same time instant. Pressure contours from CFD and DMD are plotted on the surfaces of the rod and wire and given in Fig. 5(a) and Fig. 5(b), respectively.

Finally, it is interesting to make a comparison between our results from CFD and DMD and those using high fidelity pseudo-DNS results reported by Shams et al. (2018). Fig. 6 presents the time-averaged results from three different approaches. Time averaged velocities were evaluated by averaging instantaneous results from t=2.0 s to t=3.0 s. The selected flow configuration is a complex geometry and poses challenges in understanding the local flow regimes (Bovati et al., 2022). The time averaged velocity magnitude corresponding to the mid cross-section is shown in Fig. 6(b). It can be seen that around the wire, blue regions highlight the periodic-boundary zones. However, because of the geometric design (which is compact in the cross-sectional direction), a quick transition takes place and the flow eventually develops into a highly turbulent one. The higher magnitude of the velocity appears in the narrow region between the two rods and is highlighted by the red color. It is clearly noticeable that the dominating velocity component is the Z axial velocity, represented by the W-component. Although the time averaged dimensionless velocities $\bar{U}^+$ and $\bar{V}^+$ are both lower than $\bar{W}^+$, the $\bar{U}^+$ and $\bar{V}^+$ counters shown in Fig. 6(a) which represent the secondary flow along circumferential direction of the fuel pin. The wire spacers, helically wound along the pin axis, generate the

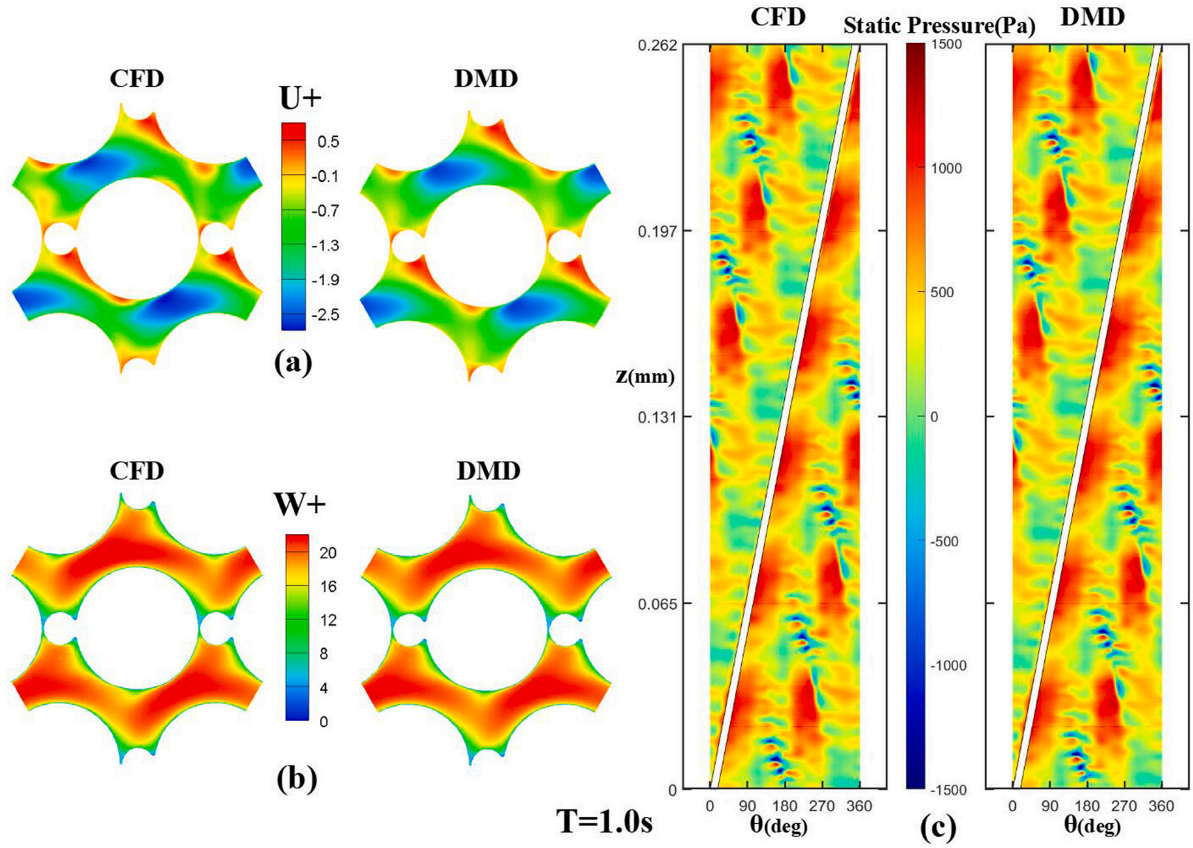

Fig. 7. Comparison of dimensionless velocity contours and pressure contours at $t = 1.0$ s in the actual service conditions. Cross-sectional views of dimensionless velocity (a) $U+$ and (b) $W+$ contours obtained from CFD simulation and DMD prediction. (c) The pressure counters given on the circumferentially expanded rod surface obtained from CFD simulation and DMD prediction.

secondary flow mentioned above. Hence the liquid LBE flow in wire-wrapped rod channel is helical pattern axial flow. Compared with the DMD time averaged dimensionless velocity $\bar{U}^+$, $\bar{V}^+$ and $\bar{W}^+$ counters in Fig. 6(a), it is obvious that DMD method can forecasting the characteristic of flow velocity field in wire-wrapped rod channel. The R^2 of time averaged dimensionless velocity $\bar{U}^+$, $\bar{V}^+$, $\bar{W}^+$ are 0.953, 0.929, 0.993, respectively, which are still acceptable. For DMD, time averaged results were obtained through reconstruction and prediction described above. Fig. 6(a) gives the cross-sectional view of three dimensionless velocities, and the cross section is also taken from the one in Fig. 1(c). In addition to the contour plots, a careful quantitative comparison is made along two lines, marked by L1 and L2 in Fig. 6(c), and the velocity profiles are plotted in Fig. 6(d). The abscissa in Fig. 6(d), S^+, is the dimensionless length and defined as $S^+ = S/D$, where S is the distance from the point on L_1 or L_2 to the center point O and D is the diameter of the rod. The dimensionless pressure drop, $\Delta P^+ = \Delta P/\tau_w$, obtained from our RANS simulation is 269.1, which is close to that by pseudo-DNS, 265.6, reported by Shams et al. (2018). Fig. 6(d) demonstrates that the overall trend of three results agree pretty well, but there still exists some discrepancy between RANS and pseudo-DNS results. This discrepancy is reasonable and owing to the intrinsic difference in accuracy between RANS and DNS and possible difference in numerical setup. Firstly, in this study, the friction velocity, U_τ, finally converges to 0.01999 for four meshes, whilst U_τ from pseudo-DNS simulation by Shams et al. (2018) is 0.0199. Secondly, it is well known that pseudo-DNS simulation outperform RANS in turbulence fluctuation capturing, and it seems that RANS underestimates wall shear stress τ_w. As a consequence, pseudo-DNS gives smaller dimensionless velocities as compared with RANS and DMD.

As the result shown in Fig. 6, the accuracy of the CFD approach and the availability of DMD prediction are demonstrated. And the LBE flow mentioned above is in the condition of low mass flow rate condition. It is necessary to carry out the CFD simulation and DMD prediction of the LBE flow in wire-wrapped rod channel with actual mass flow rate. The service conditions given by De Bruyn et al. (2013) indicated the actual mass flow rate is 1.5319 kg/s. We calculated the LBE flow in actual service condition following the previous CFD approach, and the simulation terminated at $t = 1.0$ s. The simulation process took 45 days, and it was run on computer cluster with 64 processors, each having a speed of 2.4 GHz resulting in a total computational time of ~65 thousands core hours. Three dimensionless velocity of the middle cross-section and the static pressure on the surface of fuel rod from t=0.5 s to t=0.8 s were assembled to form different snapshot matrices with time step Δt_{snap}=0.001 s. The unseen data from t=0.8 s to t=1.0 s were used for testing of DMD prediction in actual service condition. The DMD process took few minutes, it is negligible as compared with FOM modeling. In this way, the DMD method saves 20% of the time cost (the dimensionless velocity and static pressure predicted by DMD from t=0.8 s to t=1.0 s). Fig. 7 shows the comparison of dimensionless velocity contours and pressure contours at $t = 1.0$ s obtain by CFD simulation and DMD prediction. Cross-sectional views of dimensionless velocity $U+$ contours obtained from CFD simulation and DMD prediction shown in Fig. 7(a), the R^2 is 0.9534 which is satisfactory. The dimensionless velocity $U+$ in actual condition is similar to the dimensionless velocity $U+$ in low mass flow rate condition. The secondary flow along circumferential direction of the fuel pin also exists in actual service condition. The R^2 of the dimensionless velocity $W+$ is 0.998, which indicates the accuracy of the DMD prediction of LBE flow in wire-wrapped rod channel. As can be seen in Fig. 7(b), the results of the CFD simulation are in good agreement with the results of DMD prediction, and this result has further strengthened our confidence in the DMD method. Comparison between the DMD prediction and CFD result for static pressure on rod surface is represented in Fig. 7(c), the R^2 is 0.873 which is acceptable. Note that the area in front of the wire exhibits higher pressure while the area behind the wire has lower pressure, similar to the pressure distribution of LBE flow in low mass flow rate condition. But due to the higher mass flow rate in actual service condition, the amplitude of the static pressure in Fig. 7(c) is much larger than the static pressure in Fig. 3(a).

4. Conclusions

The LBE flow in wire-wrapped fuel pin bundle is complicated and fully turbulent, but is vital for heat transfer, thermal hydraulics and fluid-stricture interaction analysis of fuel assemblies using LBE as coolant. Modeling LBE flow in pin bundle is prohibitively computation-intensive, due to the highly turbulent and chaotic nature of the flow and the complicated geometry and meshing of wire-wrapped pin bundle. Yet, CFD modeling of wire-wrapped pin bundle exclusively adopts full-order modeling (FOM). Though high in accuracy, these FOM CFD simulations are extremely time and resource-consuming. The advent of data-driven reduced-order modeling (ROM) technology opens the door for accelerated simulations, the process of efficient engineering design and safety assessment of complex systems. Important conclusions from the present investigations are: 1. Using the RANS approach with stress-omega RSM turbulence model, the LBE flow in a single wire-wrapped pin channel was simulated. The complex computational domain of the unit cell was discretized by polyhedral meshes, and enforced with periodic boundary conditions. Through mesh-independence test and comparison between CFD and pseudo-DNS results in literature, the CFD approach was validated. This strategy can attain reasonable accuracy with relatively smaller number of cells, and we calculated the LBE flow with actual mass flow rate in service condition.

2. This paper reports the first reference on use of modal analysis to the turbulent LBE flow in a single wire-wrapped pin channel. The former reveals the characteristic spatial distribution of the system, while the latter reflects the temporal growth or decay of each mode. The coherent structures of the system and their evolution are helpful for gaining physical insight into the complex flow.

3. CFD simulation results on three velocities and static pressure were collected and divided into two groups: one for snapshot matrix construction and the other for testing. The process is purely data-driven and equation-free. The DMD method works fairly well in terms of flow fields reconstruction and future-state prediction, and the velocities and pressure given by DMD are validated by ground-truth CFD data, and in particular the time-averaged pseudo-DNS results in literature.

4. The data reconstruction and prediction are implemented in the context of ROM, and therefore, the computation time of ROM is negligible as compared with FOM modeling. The implementation is integrated with commercial CFD solvers and data post-processing software, and we publicly share all the codes for implementation. Our efforts open an avenue for modal analysis and ROM of complex flow in fuel assemblies as well as nuclear reactor internals.

CRediT authorship contribution statement

Xielin Zhao: Conceptualization, Methodology, Writing – review & editing, DMD. **Qian Cheng:** CFD simulation, Software. **Xiaofei Yu:** Visualization. **Qian Huang:** Investigation. **Ke Zhang:** Validation. **Zhipeng Feng:** Supervision. **Jinxiong Zhou:** Conceptualization, Writing.

Declaration of competing interest

The authors declare that they have no known competing financial interests or personal relationships that could have appeared to influence the work reported in this paper.

Data availability

Data will be made available on request.

Acknowledgments

This research is supported by National Natural Science Foundation of China (grant 11972277) and by Science and Technology on Reactor System Design Technology Laboratory (LRSDT2021205).

Appendix A. Supplementary data

Supplementary material related to this article can be found online at https://doi.org/10.1016/j.anucene.2023.109918.

References

Alemberti, A., Smirnov, V., Smith, C.F., Takahashi, M., 2014. Overview of lead-cooled fast reactor activities. Prog. Nucl. Energy 77, 300–307.
Bovati, O., Yildiz, M.A., Hassan, Y., Vaghetto, R., 2021. RANS simulations for transition and turbulent flow regimes in wire-wrapped rod bundles. Int. J. Heat Fluid Flow 90, 108838.
Bovati, O., Yildiz, M.A., Hassan, Y., Vaghetto, R., 2022. Pressure drop and flow characteristics in partially blocked wire wrapped rod bundles. Ann. Nucl. Energy 165, 108671.
Brockmeyer, L., Merzari, E., Solberg, J., Hassan, Y., 2020. One-way coupled simulation of FIV in a 7-pin wire-wrapped fuel pin bundle. Nucl. Eng. Des. 356, 110367.
Brunton, S.L., Brunton, B.W., Proctor, J.L., Kaiser, E., Kutz, J.N., 2017. Chaos as an intermittently forced linear system. Nature Commun. 8 (1), 19.
Cadiou, T., Saxena, A., 2015. Thermal–hydraulic numerical simulation of fuel sub-assembly using a dedicated meshing tool. Nucl. Eng. Des. 295, 162–172.
Chen, K.K., Tu, J.H., Rowley, C.W., 2012. Variants of dynamic mode decomposition: boundary condition, koopman, and Fourier analyses. J. Nonlinear Sci. 22, 887–915.
De Bruyn, D., Abderrahim, H.A., Baeten, P., Fernandez, R., Van den Eynde, G., 2013. Recent design developments of the MYRRHA ADS project in Belgium. In: Proceedings of ICAPP. pp. 14–18.
De Pauw, B., Lamberti, A., Ertveldt, J., Rezayat, A., Van Tichelen, K., Vanlanduit, S., Berghmans, F., 2016. Vibration monitoring using fiber optic sensors in a lead-bismuth eutectic cooled nuclear fuel assembly. Sensors 16 (4), 571.
De Santis, D., Shams, A., 2019. Analysis of flow induced vibrations and static deformations of fuel rods considering the effects of wire spacers and working fluids. J. Fluids Struct. 84, 440–465.
Dolfen, H., De Ridder, J., Brockmeyer, L., Merzari, E., Kennedy, G., Van Tichelen, K., Degroote, J., 2022. A multi-stage approach of simulating turbulence-induced vibrations in a wire-wrapped tube bundle for fretting wear prediction. J. Fluids Struct. 109, 103460.
Dovizio, D., Mikuž, B., Shams, A., Roelofs, F., 2020. Validating RANS to predict the flow behavior in wire-wrapped fuel assemblies. Nucl. Eng. Des. 356, 110376.
Kamb, M., Kaiser, E., Brunton, S.L., Kutz, J.N., 2020. Time-delay observables for koopman: Theory and applications. SIAM J. Appl. Dyn. Syst. 19 (2), 886–917.
Kennedy, G., Van Tichelen, K., Doolaard, H., 2015. Experimental investigation of the pressure loss characteristics of the full-scale MYRRHA fuel bundle in the COMPLOT LBE facility. In: International Topical Meeting on Nuclear Reactor Thermal Hydraulics 2015, Vol. 1. NURETH 2015, pp. 61–73.
Kutz, J.N., Brunton, S.L., Brunton, B.W., Proctor, J.L., 2016. Dynamic Mode Decomposition: Data-Driven Modeling of Complex Systems. SIAM.
Merzari, E., Cheung, F.-B., Bajorek, S.M., Hassan, Y., 2021. 40th Anniversary of the first international topical meeting on nuclear reactor thermal-hydraulics: Highlights of thermal-hydraulics research in the past four decades. Nucl. Eng. Des. 373, 110965.
Merzari, E., Fischer, P., Yuan, H., Van Tichelen, K., Keijers, S., De Ridder, J., Degroote, J., Vierendeels, J., Doolaard, H., Gopala, V., et al., 2016. Benchmark exercise for fluid flow simulations in a liquid metal fast reactor fuel assembly. Nucl. Eng. Des. 298, 218–228.
Mezić, I., 2005. Spectral properties of dynamical systems, model reduction and decompositions. Nonlinear Dynam. 41 (1), 309–325.
Mezić, I., 2013. Analysis of fluid flows via spectral properties of the koopman operator. Annu. Rev. Fluid Mech. 45, 357–378.
Mezić, I., Banaszuk, A., 2004. Comparison of systems with complex behavior. Physica D 197 (1–2), 101–133.
Naderi, M.H., Eivazi, H., Esfahanian, V., 2019. New method for dynamic mode decomposition of flows over moving structures based on machine learning (hybrid dynamic mode decomposition). Phys. Fluids 31 (12), 127102.
Nixon, C.A., 2018. On the flow-induced vibration of solitary wire-wrapped cylinders in axial flow.
Roelofs, F., 2020. Liquid metal thermal hydraulics: state-of-the-art and future perspectives. Nucl. Eng. Des. 362, 110590.

Rowley, C.W., Mezić, I., Bagheri, S., Schlatter, P., Henningson, D.S., 2009. Spectral analysis of nonlinear flows. J. Fluid Mech. 641, 115–127.

Schmid, P.J., 2010. Dynamic mode decomposition of numerical and experimental data. J. Fluid Mech. 656, 5–28.

Schmid, P.J., 2022. Dynamic mode decomposition and its variants. Annu. Rev. Fluid Mech. 54, 225–254.

Schmid, P., Sesterhenn, J., 2008. Dynamic mode decomposition of numerical and experimental data. Bull. Am. Phys. Soc. 53.

Shams, A., Roelofs, F., Baglietto, E., Komen, E., 2018. High fidelity numerical simulations of an infinite wire-wrapped fuel assembly. Nucl. Eng. Des. 335, 441–459.

Taira, K., Brunton, S.L., Dawson, S.T., Rowley, C.W., Colonius, T., McKeon, B.J., Schmidt, O.T., Gordeyev, S., Theofilis, V., Ukeiley, L.S., 2017. Modal analysis of fluid flows: An overview. AIAA J. 55 (12), 4013–4041.

Tu, J.H., 2013. Dynamic Mode Decomposition: Theory and Applications (Ph.D. thesis). Princeton University.

Van Tichelen, K., Kennedy, G., Mirelli, F., Marino, A., Toti, A., Rozzia, D., Cascioli, E., Keijers, S., Planquart, P., 2020. Advanced liquid-metal thermal-hydraulic research for MYRRHA. Nucl. Technol. 206 (2), 150–163.

Wilcox, D.C., et al., 1998. Turbulence Modeling for CFD, Vol. 2. DCW industries La Canada, CA.

Yildiz, M.A., Merzari, E., Hassan, Y.A., 2019. Spectral and modal analysis of the flow in a helical coil steam generator experiment with large eddy simulation. Int. J. Heat Fluid Flow 80, 108486.

Zhao, X., Guo, R., Yu, X., Huang, Q., Feng, Z., Zhou, J., 2022. Dynamic mode decomposition for data-driven modeling of free surface sloshing. Modern Phys. Lett. B 36 (19), 2250036.